Make the Most of Time

Temporal Extension of the iTV Algorithm for 4D Cardiac C-Arm CT

Viktor Haase[1,5], Oliver Taubmann[2,3], Yixing Huang[2], Gregor Krings[4], Günter Lauritsch[5], Andreas Maier[2,3], Alfred Mertins[1]

[1]Institute for Signal Processing, University of Luebeck
[2]Pattern Recognition Lab, Friedrich-Alexander-University Erlangen-Nuremberg
[3]Graduate School in Advanced Optical Technologies (SAOT), Erlangen, Germany
[4]University Medical Center Utrecht, Netherlands
[5]Siemens Healthcare GmbH, Forchheim, Germany
viktor.haase@student.uni-luebeck.de

Abstract. Gated 4D cardiac imaging with C-arm CT scanners suffers from insufficient image quality due to strong angular undersampling. To deal with this problem, we suggest an iterative reconstruction method with spatial and temporal total variation regularization based on an established framework which controls the relative contributions of raw data error minimization and regularization. This new method is tested on a simulated heart phantom and on two clinical data sets. We show that the additional use of temporal regularization is advantageous compared to spatial regularization exclusively, with the relative root mean square error lowered from 11.75 % to 8.24 % in the phantom study.

1 Introduction

Tomographic medical image generation by an angiographic C-arm system during an intervention would be efficient and helpful for planning, guiding and monitoring the therapeutic procedure. The research efforts of the last few years make it possible to reconstruct four-dimensional (4D) volumes using C-arm scanners [1, 2]. The projection data of one C-arm rotation documents various cardiac phases of multiple heart beats. ECG-gating, which divides the projection data into subsets for individual heart phases, is necessary to achieve sufficient temporal resolution. Each resulting subset contains too few projections and thereby allows only a highly artifact-impaired 3D image reconstruction. Therefore, 4D cardiac imaging typically suffers from bad image quality.

To overcome these problems, motion estimation and compensation algorithms are suggested in the framework of filtered backprojection reconstruction techniques [1, 2]. Further improvements are achieved by incorporating spatio-temporal smoothing [3]. The problem of undersampled data is also addressed by iterative optimization algorithms in the context of compressed sensing. They employ sparsity-based regularization such as spatial total variation (TV) minimization. Mory et al. add a temporal TV regularizer for 4D cardiac imaging,

T. Tolxdorff et al. (Hrsg.), *Bildverarbeitung für die Medizin 2016*,
DOI 10.1007/978-3-662-49465-3_31,

achieving superior image results [4]. By applying temporal regularization, information of data from all heart phases can be leveraged during reconstruction of each individual phase. The improved total variation (iTV) algorithm [5] is a sophisticated implementation of a spatial TV regularized reconstruction in which the trade-off of data fidelity and spatial regularization is controlled adaptively, in contrast to a fixed balance as used in, e. g., Mory's algorithm [4]. In this paper, we propose to extend the iTV algorithm in order to incorporate temporal regularization.

2 Materials and methods

The iTV algorithm uses the simultaneous algebraic reconstruction technique (SART) and spatial TV minimization in an alternating manner [5]. In this section, we explain our adjustments to iTV and specify the data used for evaluation.

2.1 Image reconstruction with spatio-temporal regularization

For 4D imaging several cardiac phases $t \in T = \{0, \ldots, N_{\text{phases}}\}$ are reconstructed. The measured projection data $\boldsymbol{p}(t)$ are assigned a heart phase t, with $\boldsymbol{f}_n(t)$ denoting the corresponding reconstruction after iteration $n \in \{1, \ldots, N\}$.

An overview of our method is given in Fig. 1. We start from an empty volume $\boldsymbol{f}_0(t) = \boldsymbol{0}$. To ensure data fidelity, a SART update step including a non-negativity constraint is calculated in the beginning of each iteration resulting in the volume $\boldsymbol{f}_{n+1}^{\text{SART}}(t)$. Two temporal regularization steps (orange boxes in Fig. 1) are introduced in addition to the spatial TV minimization of the original iTV algorithm. At first, a no-motion constraint is enforced outside of a (manually chosen) volume of interest (VOI) containing the heart to improve convergence [4]. For this purpose, all voxels outside of the VOI are averaged over the temporal domain. Then, spatial TV minimization is applied to each volume [5]. Next, temporal TV regularization is incorporated into the algorithm, extending the idealized assumption of piecewise constant objects to the temporal domain. The 1D TV norm w. r. t. the temporal domain [4] is calculated. It is minimized for

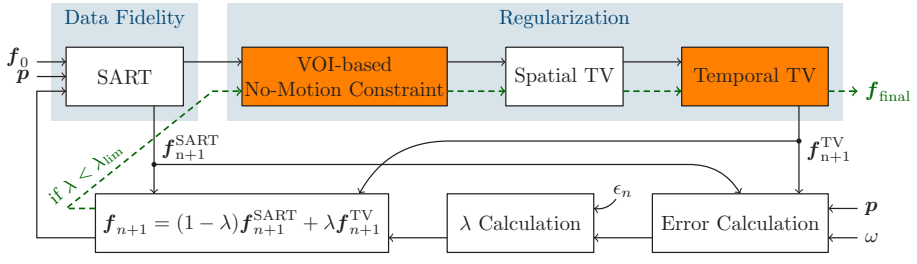

Fig. 1. Sequence diagram of the extended iTV algorithm. The new temporal regularization parts are highlighted in orange. When the stopping criterion $\lambda < \lambda_{\text{lim}}$ is reached, $\boldsymbol{f}_{\text{final}}(t)$ is calculated using the dashed green path.

all voxels simultaneously by gradient descent iterations using backtracking line search and "corner rounding" to enable discrete differentiability. We denote the resulting volumes as $\boldsymbol{f}_{n+1}^{\mathrm{TV}}(t)$.

So as not to abandon raw data fidelity in spite of the desired regularization, $\boldsymbol{f}_{n+1}^{\mathrm{SART}}(t)$ and $\boldsymbol{f}_{n+1}^{\mathrm{TV}}(t)$ are combined linearly at the end of each iteration [5]

$$\boldsymbol{f}_{n+1}(t,\lambda) = (1-\lambda)\boldsymbol{f}_{n+1}^{\mathrm{SART}}(t) + \lambda \boldsymbol{f}_{n+1}^{\mathrm{TV}}(t) \tag{1}$$

The variable $\lambda \in [0,1]$ controls the impact of data fidelity and regularization. We design it to be independent of the heart phase, thereby avoiding different degrees of smoothing applied to the individual phases. It is related to the parameter $\omega \in]0,1[$ which specifies the permitted loss of data consistency by regularization for the current iteration $n+1$ regarding the previous n-th iteration

$$\epsilon_{n+1} = (1-\omega)(\epsilon_{n+1}^{\mathrm{SART}} - \epsilon_n) + \epsilon_n \tag{2}$$

where ϵ now denotes the total data consistency error for all phases

$$\epsilon = \sum_{t \in T} (\|R(t)\boldsymbol{f}(t,\lambda) - \boldsymbol{p}(t)\|_2^2) \tag{3}$$

$R(t)$ is the system matrix that describes the projection of $\boldsymbol{f}(t)$ to the corresponding raw data $\boldsymbol{p}(t)$. By solving the quadratic Eq. (2), the ideal λ is determined [5]. If this would result in $\lambda < 0$ or $\lambda > 1$, λ is set back to its defined limits.

Typically, λ starts at 1 and decreases over the course of optimization [5]. Instead of a fixed maximum number of iterations N, we prefer to stop the reconstruction after λ has dropped below a specified limit λ_{lim}. Hence, the desired degree of smoothness in the resulting images can be specified directly. Higher values of λ_{lim} lead to a more comic-like appearance due to stronger TV minimization. With a high ω, the λ values decrease more slowly, resulting in more iterations to be performed. Once the stopping criterion is reached, the full regularization is applied one last time (visualized as the green path in Fig. 1) so that high-frequency artifacts are reduced in the final volume $\boldsymbol{f}_{\mathrm{final}}(t)$.

2.2 Experimental setup

The reconstruction method is evaluated on a simulated heart phantom data set [6]. The projections are generated with a polychromatic X-ray spectrum [7]. The acquisition protocol is identical to that of the clinical data sets described below, with a simulated heart rate of 120 bpm and no respiratory motion. The ground truth is a static phantom showing the end-diastolic heart phase. It is reconstructed from a fully sampled scan with our method (Fig. 2 (a)). As evaluation measures, the relative root mean square error (RMSE) and the universal image quality index (UQI) [8] are calculated over the VOI. Instead of a global computation, the UQI is averaged over 10 small blocks of size $(16\,\mathrm{mm})^3$ to increase sensitivity.

To test our proposed algorithm on real data, two clinical patient data sets are acquired using an Artis zee biplane system (Siemens Healthcare GmbH, Forchheim, Germany). The detector dimension is 960 x 960 pixels. The isotropic pixel resolution is 0.312 mm/pixel (0.21 mm/pixel in isocenter). One C-arm rotation of 5 s duration is performed, capturing 133 projection images with an angular increment of 1.5° per frame. The heart is paced through external stimulation to 228 bpm for the first and 140 bpm for the second data set, resulting in 19 and 11 heartbeats per rotation, respectively.

The following reconstruction parameters are used: For all data sets, eight cardiac phases are reconstructed. In every SART update step, eight full SART subiterations are executed with a relaxation parameter of 0.8. Every SART subset consists of one complete projection image. For both TV minimization steps, 10 gradient descent iterations are performed. The chosen values for the convergence controlling parameters $\omega = 0.8$ and $\lambda_{\text{lim}} = 0.35$ are determined empirically.

To bring out the effects of our proposed method more clearly, all reconstructions are repeated with spatial TV minimization only, excluding the temporal regularization steps.

3 Results

The results for the heart phantom data set are shown in Fig. 2. For the sake of comparison, a SART reconstruction without any regularization is performed

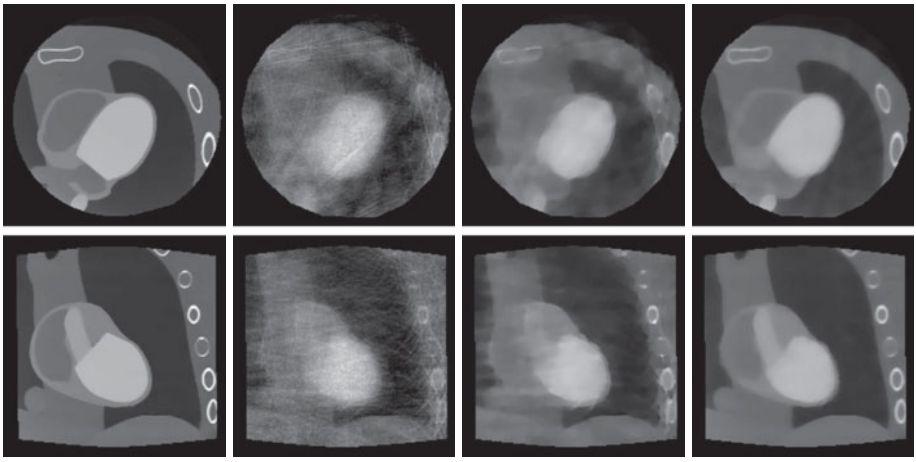

(a) (b) (c) (d)

Fig. 2. Reconstructed images of the heart phantom data set. From left to right: Ground truth (a), SART reconstruction (b), iterative reconstruction with spatial TV regularization (c) and our proposed method (d). All images display the end-diastolic heart phase. The top row shows an axial plane, a coronal plane is depicted underneath. The grayscale is set to $[-1000, 2480]$ HU.

(Fig. 2(b)). The image is dominated by noise and streaks due to undersampling and the process is stopped after 10 iterations as no further improvement is identified after this point. To a certain degree, these artifacts can be reduced by applying spatial TV regularization as seen in Fig. 2(c). The image quality achieved with our proposed spatio-temporal regularization in Fig. 2(d) is a pronounced improvement; all structures seen in the ground truth (Fig. 2(a)) are now represented more clearly, even though they are somewhat blurred. For the heart itself, this may in part be caused by residual motion inside the gating window.

The visual advantages of the incorporated temporal regularization compared to the application of spatial regularization only are reflected by the quantitative evaluation. The relative RMSE over the VOI is decreased from 11.75 % to 8.24 % and the UQI over the VOI is increased from 0.76 to 0.98. Fig. 3 shows that the temporal regularization helps to accelerate the convergence of the reconstruction as λ reaches the lower limit of λ_{lim} more quickly. Instead of 63 iterations, only 22 iterations are necessary to achieve convergence.

The spatio-temporal regularization also works well on our clinical data. A clear improvement can be seen for the first data set in Fig. 4(b) compared to 4(a) as well as for the second in Fig. 4(d) compared to 4(c). In general, the reconstruction of the second data set struggles with more artifacts due to the lower number of recorded heart beats. It took 18 iterations for the first and 19 iterations for the second data set to converge with our proposed method.

4 Discussion

While the chosen parameters appear to be suitable for the examined data sets, it is yet to be verified how well they generalize over a larger number of cases. As an extension of the proposed method, it may be helpful to introduce the possibility to control the influence of the temporal TV minimization separately from the spatial one. For further research, it may be worthwhile to implement a different optimization algorithm which does not optimize the data fidelity and regularization terms alternately but combines them into one cost function to minimize them jointly as proposed in [9].

We suggest an extended version of the iTV algorithm using spatio-temporal regularization to overcome the challenges posed by angular undersampling due to ECG gating. The results of our experiments in a phantom study and on two clinical data sets demonstrate that especially the use of temporal regularization is highly beneficial for use in 4D cardiac C-arm CT.

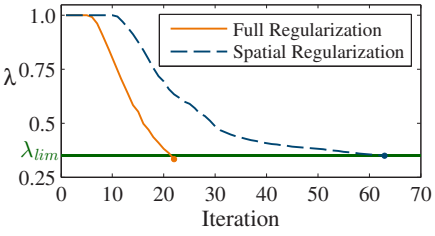

Fig. 3. Development of λ during the reconstruction of the phantom data set. The spatial regularization (dashed blue curve) is compared to the proposed spatio-temporal regularization (orange curve). The threshold λ_{lim} used in our stopping criterion is marked with the green line.

Fig. 4. Reconstructed images of the clinical patient data sets. From left to right: the first data set reconstructed with spatial TV regularization (a) and with our proposed method (b), the second data set reconstructed with spatial TV regularization (c) and with our proposed method (d). All images show a coronal view. The grayscale is set to $[-1000, 2480]$ HU.

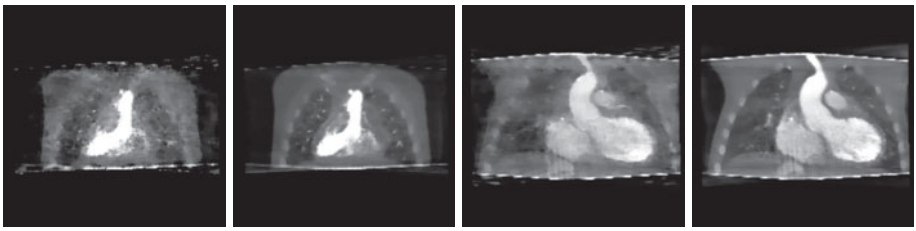

(a) (b) (c) (d)

Disclaimer. The concepts and information presented in this paper are based on research and are not commercially available.

References

1. Müller K, Maier A, Schwemmer C, et al. Image artefact propagation in motion estimation and reconstruction in interventional cardiac C-arm CT. Phys Med Biol. 2014;59(12):3121.
2. Wielandts JY, De Buck S, Michielsen K, et al. Multi-phase rotational angiography of the left ventricle to assist ablations: feasibility and accuracy of novel imaging. Eur Heart J - Cardiovasc Imaging. 2015.
3. Taubmann O, Lauritsch G, Maier A, et al. Estimate, compensate, iterate: joint motion estimation and compensation in 4-D cardiac C-arm computed tomography. Proc MICCAI. 2015; p. 579–86.
4. Mory C, Auvray V, Zhang B, et al. Cardiac C-arm computed tomography using a 3D + time ROI reconstruction method with spatial and temporal regularization. Med Phys. 2014;41(2):021903.
5. Ritschl L, Bergner F, Fleischmann C, et al. Improved total variation-based CT image reconstruction applied to clinical data. Phys Med Biol. 2011;56(6):1545.
6. Segars W, Sturgeon G, Mendonca S, et al. 4D XCAT phantom for multimodality imaging research. Med Phys. 2010;37(9):4902–15.
7. Maier A, Hofmann HG, Berger M, et al. CONRAD - A software framework for cone-beam imaging in radiology. Med Phys. 2013;40(11):111914.
8. Wang Z, Bovik AC. A universal image quality index. IEEE Signal Process Lett. 2002;9(3):81–4.
9. Lauzier PT, Tang J, Chen GH. Prior image constrained compressed sensing: implementation and performance evaluation. Med Phys. 2012;39(1):66–80.